Engineering Structures 151 (2017) 349–365

Contents lists available at ScienceDirect

Engineering Structures

journal homepage: www.elsevier.com/locate/engstruct

Simulating masonry wall behaviour using a simplified micro-model approach

Kurdo F. Abdulla [a,*], Lee S. Cunningham [a], Martin Gillie [b]

[a] Mechanical, Aerospace and Civil Engineering School, The University of Manchester, Oxford Road, Manchester M13 9PL, United Kingdom
[b] School of Engineering, University of Warwick, Coventry CV4 7AL, United Kingdom

ARTICLE INFO

Article history:
Received 6 December 2016
Revised 10 August 2017
Accepted 12 August 2017

Keywords:
Modelling masonry
Surface-based cohesive behaviour
XFEM
Crack propagation
In-plane load
Out of plane load
Cyclic in-plane load

ABSTRACT

In this paper, a simplified micro-model approach utilising a combination of plasticity-based constitutive models and the extended finite element method (XFEM) is proposed. The approach is shown to be an efficient means of simulating the three-dimensional non-linear behaviour of masonry under monotonic in-plane, out of plane and cyclic loads. The constitutive models include surface-based cohesive behaviour to capture the elastic and plastic behaviour of masonry joints and a Drucker Prager (DP) plasticity model to simulate crushing of masonry under compression. The novel use of XFEM in simulating crack propagation within masonry units without initial definition of crack location is detailed. Analysis is conducted using standard finite element software (Abaqus 6.13) following a Newton Raphson algorithm solution without employing user-defined subroutines. The capability of the model in terms of capturing non-linear behaviour and failure modes of masonry under vertical and horizontal loads is demonstrated via comparison with a number of published experimental studies.

1. Introduction

Masonry is one of the oldest and most widespread structural materials; it has been and is still used for various construction purposes. Masonry consists of units and mortar, these constituents have their own mechanical properties and their geometry and arrangement can vary forming different masonry assemblages. Thus masonry is classified as a heterogeneous anisotropic material, and analysis, understanding and capture of the structural behaviour of masonry is therefore complex. For design of non-standard masonry structures or assessment of existing structures, recourse to numerical modelling is often required to understand the structural behaviour under various loading conditions.

Nowadays, numerical models offer a viable alternative to physical experiments. Different numerical methods such as the finite element method (FEM), discrete element method (DEM), limit analysis [1,2] and the applied element method (AEM) [3] have been employed to conduct numerical analysis and simulate linear and non-linear behaviour of masonry. The finite element method (FEM) is the focus of this paper. FEM for masonry is based on two main modelling approaches, namely, Micro-modelling and Macro-modelling, the choice depending on the level of accuracy and detail required.

In the Micro-model approach, the simulation can be detailed; the units and mortar are modelled as continuum elements and unit-mortar interfaces are modelled as discontinuum elements. The detailed Micro-model Fig. 1(a) can provide accurate results, but it is computationally intensive and thus limited to simulating relatively small masonry elements. Alternatively, a simplified Micro-modelling approach Fig. 1(b) can be adopted to address the disadvantages of the detailed micro approach. In the simplified approach, the units are expanded by adding the mortar thickness, the expanded units are modelled as a series of continuum elements and the interaction between the expanded units is modelled as series of discontinuum elements.

In the Macro-model approach, Fig. 1(c), the masonry is considered as a homogenous material with no distinction between units and mortar, the material properties are obtained from average properties of masonry constituents and the masonry is modelled as a series of continuum elements [4]. This approach is adopted where relatively larger and more complex masonry structures are modelled and the global behaviour is of interest, but it cannot capture detailed failure modes.

Over the past four decades, finite element techniques have continuously evolved to capture the complex structural behaviour of masonry walls and associated structures. Arya and Hegemier [5]

* Corresponding author.
E-mail address: kurdo.abdulla@manchester.ac.uk (K.F. Abdulla).

http://dx.doi.org/10.1016/j.engstruct.2017.08.021
0141-0296/

Nomenclature

c	cohesion between the masonry joints interfaces (MPa)
D	damage evolution variable
d	material cohesion (MPa)
E_{adj}	adjusted elastic modulus (MPa)
E_m	elastic modulus of mortar (MPa)
E_u	elastic modulus of units (MPa)
f_{mt}	flexural tensile strength of masonry (MPa)
G_m	shear modulus of mortar (MPa)
G_u	shear modulus of units (MPa)
G_I	work done by the traction-separation in the normal direction (N/mm)
G_{II}	work done by the traction-separation in the first shear direction (N/mm)
G_{III}	work done by the traction-separation in the second shear direction (N/mm)
G_{TC}	critical mixed-mode energy dissipation at failure (N/mm)
G_{IC}	critical fracture energy in the normal direction, refers to as mode I fracture energy (N/mm)
G_{IIC}	critical fracture energy in the first and second shear directions, refers to as mode II and mode III fracture energies (N/mm)
H	height of masonry assemblage (mm)
h_m	thickness of mortar (mm)
h_u	height of masonry unit (mm)
$\mathbf{I}$	identity matrix
$\boldsymbol{K}$	elastic stiffness matrix
K_{nn}	stiffness of masonry joints in the normal direction (N/mm^3)
K_{ss}	stiffness of masonry joints in the first shear direction (N/mm^3)
K_{tt}	stiffness of masonry joints in the second shear direction (N/mm^3)
k_b	numerical factor
l_u	length of masonry units (mm)
M_d	diagonal bending moment capacity of masonry (N mm/mm)
M_h	horizontal bending moment capacity of masonry (N mm/mm)
n	number of courses in a masonry assemblage
R	ratio of the yield stress in triaxial tension to the yield stress in triaxial compression (flow stress ratio)
r	third invariant of deviatoric stress (MPa)
$\mathbf{S}$	stress deviator (MPa)
$\boldsymbol{t}$	nominal traction stress vector
t_u	thickness of masonry units (mm)
t^o_{eff}	effective traction stress at damage initiation under combinations of normal and shear tractions in the joints (MPa)
t_n	normal traction stress in masonry joints in the normal direction (MPa)
t_s	shear traction stress in masonry joints along the first shear direction (MPa)
t_t	shear traction stress in masonry joints along the second shear direction (MPa)
t_n^{max}	maximum allowable traction stress in masonry joints in the normal direction (Tensile strength of masonry joints) (MPa)
t_s^{max}	maximum allowable traction stress in masonry joints in the first shear direction (Shear strength of masonry joints) (MPa)
t_t^{max}	maximum allowable traction stress in masonry joints in the second shear direction (Shear strength of masonry joints) (MPa)
β	material friction angle (Degree)
δ	separation vector
δ_{eff}	effective separation (mm)
δ_n^o	separation of masonry joints at the initiation of damage in the normal direction (mm)
δ_s^o	separation of masonry joints at the initiation of damage in the first shear direction (mm)
δ_t^o	separation of masonry joints at the initiation of damage in the second shear direction (mm)
δ_n^f	separation of masonry joints at the complete failure in the normal direction (mm)
δ_s^f	separation of masonry joints at the complete failure in the first shear direction (mm)
δ_t^f	separation of masonry joints at complete failure in the second shear direction (mm)
η	exponent in the BK law associated with cohesive property i.e. brittle, ductile, etc.
μ	coefficient of friction between the masonry joints interfaces
v	Poisson's ratio
$\boldsymbol{\sigma}$	stress tensor
σ_c	compressive yield stress of masonry assemblage (MPa)
σ_n	normal contact pressure stress in masonry joint interfaces (MPa)
$\boldsymbol{\tau}_{crit}$	critical shear stress in masonry joint interfaces at which interfaces fail (MPa)
$\boldsymbol{\tau}_{sliding}$	post-failure shear stress in masonry joint interfaces at which interfaces slide (MPa)
$\varnothing$	gle of diagonal crack line in masonry under out of plane loading (Degree)
ψ	dilation angle (Degree)

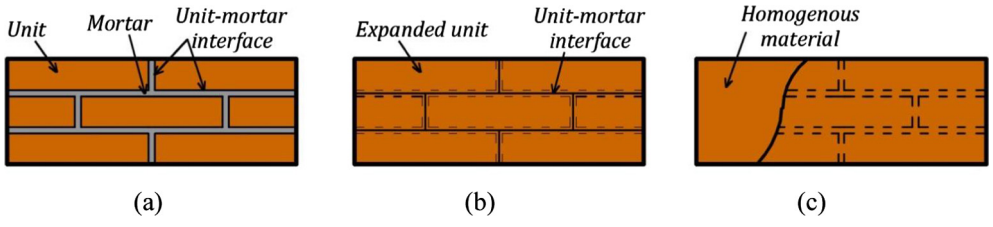

Fig. 1. Finite element modelling approaches: (a) detailed Micro-model; (b) simplified Micro-model; (c) Macro-model (based on [4]).

and Page [6] attempted to model masonry using a simplified Micro-modelling approach by taking masonry units as continuum elements and mortar joints as interface elements. This approach was then adopted by Lotfi and Shing [7] to study the behaviour of masonry assemblages by including the fracture of the mortar joints into the model via interface elements. The crack initiation and evolution of masonry mortar joints were successfully simulated under combined normal and shear stresses in both tension-shear and compression-shear regions, but the simulation of masonry was not successful under high compression stress. Lourenço and Rots [8] developed a multi-surface interface model which is defined based on three yield functions, namely, a tension cut-off for tensile failure, a Mohr-Coulomb failure envelop for shear failure and a cap model for compressive failure. In addition, potential vertical cracks were placed in the middle of the masonry units which allowed the simulation of vertical cracks under pure tension.

Shing and Cao [9] conducted finite element analysis for partially grouted masonry shear walls, a smeared crack model was adopted to simulate the fracture behaviour of the masonry units and plasticity-based interface elements were used to simulate the mortar joint responses under tensile and shear stress. Although, the model successfully simulated the failure modes of the masonry walls, the lateral resistance of the walls was higher than the resistance obtained from experiments. For example in one of the models reported, the lateral resistance from the numerical analysis was 60% higher than the experimental results. Sutcliffe et al. [10] conducted a lower bound limit analysis for masonry shear walls where both tensile and shear failure in the brick units and a compression cap for the interface elements were included, but material softening behaviour was ignored. Citto [11] and Kumar et al. [12] developed an interface model to simulate initiation and propagation of cracks in masonry joints and potential vertical cracks in the middle of masonry units under normal and shear stresses, a compression cap was also included in the model to simulate the plastic response under compression. The proposed model in [11,12] was analysed via Abaqus by making use of a user defined subroutine, which defined the constitutive behaviour. In all the aforementioned studies, simplified 2D Micro-models were used to simulate only in-plane behaviour of masonry under normal and shear stresses.

The aforementioned studies have dealt with monotonic in-plane load regimes. With regards to modelling cyclic in-plane loading of masonry, a study conducted by Oliveira and Lourenço [13], proposed a 2D model to simulate the behaviour of masonry under cyclic loadings using interface elements between masonry units. In a more recent study conducted by Miglietta et al. [14], finite/discrete element modelling (DEM) is implemented to simulate the behaviour of masonry under reversed cyclic in-plane loadings. The implemented 2D model depended on stress-displacement relationships between the adjacent masonry elements to simulate the opening and sliding behaviour of masonry joint elements. The model was shown to be capable of capturing the response and failure modes of masonry under reversed cyclic in-plane loadings. However, the crushing of masonry under compression, which is a possible failure mode of masonry under cyclic loads, was not considered.

Several studies have also been undertaken to simulate the behaviour of masonry under monotonic out of plane loads. Kuang and Yuen [15] conducted a 3D explicit-dynamic numerical analysis through a damage based cohesive crack model. The model was implemented in Abaqus via a user defined subroutine, which defined the interaction between the masonry units' surfaces. The model was capable of capturing non-linear response and failure modes of masonry infilled reinforced concrete frames under combined in-plane, out of plane and dynamic loads. However, the crushing of masonry in compression and cracking of masonry units was not considered in the model.

La Mendola et al. [16] undertook a finite element analysis to simulate non-linear out of plane behaviour of masonry. The analysis was conducted by employing interface elements with a bilinear law to simulate crack initiation and propagation in the masonry joints. The crack formations in the joints were in good agreement with experimental results; however masonry components were modelled using an isotropic linear elastic law where a possible compressive failure mechanism was not taken into consideration. Aref and Dolatshahi [17] developed a 3D constitutive material model with an explicit-dynamic analysis procedure in Abaqus. The model was defined through a user-defined subroutine to capture the linear and non-linear behaviour of masonry under in-plane, out-of-plane and cyclic loadings.

In summary, most of the existing masonry numerical analysis studies have focused on 2D analysis which is limited to simulating unreinforced masonry under normal and shear stresses, and possibly through-thickness out of plane behaviour. Realistic, 3D models are required to conduct masonry FE analysis under more complicated loading conditions such as the combined in-plane and out of plane loads associated with in service conditions. Furthermore, 3D models are necessary to simulate reinforced masonry walls because simulation is either not possible or limited in 2D FE analysis. A few of the proposed 3D models available in the literature such as in [15,17] have relied on employing a user subroutine and an explicit dynamic analysis procedure. In addition, it can be noted that the crack propagation in the brick units, which plays an important role in non-linear degradation of masonry assemblages, is either ignored or defined via interface elements. In the latter case, the formation of potential cracks has always been assumed to be vertical in the middle of units.

This paper presents a simplified 3D Micro-modelling approach to simulating the 3D behaviour of masonry. The modelling approach is implemented using the commercially available FE package, Abaqus. A combined 3D finite element model is proposed to simulate masonry walls under monotonic in-plane, out of plane and cyclic in-plane loads using a quasi-static solution procedure. The model relies on: surface based cohesion with two yield criteria (tensile and shear) to simulate crack initiation and propagation of masonry joints, and a Drucker Prager plasticity model to capture crushing of masonry under compression. The implemented model is novel in that:

- It simulates the detailed behaviour of masonry walls under in-plane and out of plane loads using quasi-static analyses.
- In contrast to the all previous approaches, it captures crack propagation within masonry units without requiring initial definition of crack location by using the extended Finite Element Method (XFEM).
- The proposed model is simplified and user friendly since it is developed by making use of methods available in the Abaqus Library without employing any user defined subroutines.

2. Modelling approach

Herein the constitutive models used to simulate 3D masonry under the simplified modelling approach are described in detail. In addition, the failure modes associated with the models are also presented.

2.1. Surface-based cohesive behaviour model

This surface-based cohesive model is employed to obtain the structural response of masonry along bed and head joints. In other words, linear and fracture behaviour of joints which is based on traction separation behaviour between masonry units, is captured. Thus, failure modes of masonry joints, namely, tensile cracking of

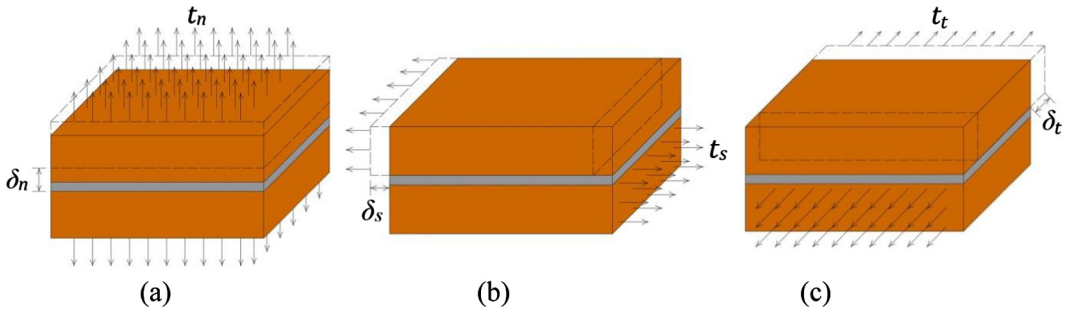

Fig. 2. Failure modes of the joints: (a) tensile cracking; (b) and (c) shear sliding.

the joints Fig. 2(a) and shear sliding of the joints Fig. 2(b) and (c) are simulated.

2.1.1. Elastic response of the joint interfaces

The initial response of the joint interfaces is based on a linear traction separation relationship prior to damage. The general linear behaviour is written in the form of an elastic stiffness matrix. The relation between the elastic stiffness matrix $\boldsymbol{K}$, nominal traction vector $\boldsymbol{t}$, and corresponding separation vector $\boldsymbol{\delta}$, of the joint interfaces Fig. 3 is expressed as in Eq. (1)

$$\boldsymbol{t} = \begin{Bmatrix} t_n \\ t_s \\ t_t \end{Bmatrix} = \begin{bmatrix} K_{nn} & 0 & 0 \\ 0 & K_{ss} & 0 \\ 0 & 0 & K_{tt} \end{bmatrix} \begin{Bmatrix} \delta_n \\ \delta_s \\ \delta_t \end{Bmatrix} = \boldsymbol{K}\ \boldsymbol{\delta} \tag{1}$$

The components of stiffness matrix $\boldsymbol{K}$, for joint interfaces in a simplified masonry Micro-model (interfaces between expanded masonry units) should be equivalent to the stiffness of the original masonry joint interfaces (brick and mortar) under the same boundary conditions. So, the equivalent stiffness for joint interfaces is expressed as a function of the mortar's and unit's moduli of elasticity, and the thickness of the mortar Eqs. (2) and (3) [4].

$$K_{nn} = \frac{E_u E_m}{h_m(E_u - E_m)} \tag{2}$$

$$K_{ss}\ and\ K_{tt} = \frac{G_u G_m}{h_m(G_u - G_m)} \tag{3}$$

2.1.2. Plastic response of the joint interfaces

The initial linear response of the joints is followed by crack propagation. When the damage initiation criterion is achieved based on the user defined tractions between the masonry interfaces i.e. shear and tensile strength of the joints, cracking propagates in the masonry joints. The quadratic stress criterion is used to define damage initiation; this criterion is met when the quadratic stress ratios of masonry interfaces are equal to one. This criterion is adopted as it effectively predicts the damage initiation of joints subjected to mixed-mode loadings [18], which is the case in masonry joint interfaces (the masonry joint interfaces are subjected to tensile stress in the normal direction and shear stress in the two shear directions). The criterion is expressed as in Eq. (4).

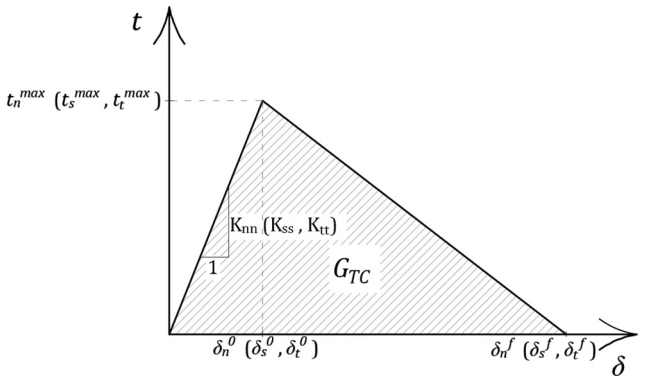

Fig. 3. Traction separation response of masonry joint interfaces in tension and shear.

$$\left(\frac{\langle t_n \rangle}{t_n^{max}}\right)^2 + \left(\frac{t_s}{t_s^{max}}\right)^2 + \left(\frac{t_t}{t_t^{max}}\right)^2 = 1 \tag{4}$$

The Macaulay bracket in Eq. (4) indicates the exclusion of the compressive stresses on the fracture behaviour of the joints in the normal direction. Tensile cracking of masonry joints is governed by the defined tensile strength of masonry joints. Critical shear stress of joints prior to failure is described by Mohr-Coulomb failure Eq. (5).

$$\tau_{crit} = c + \mu\sigma_n \tag{5}$$

The shear strength of masonry joints is calculated based on Eq. (5), in which the cohesion, coefficient of friction and normal compressive stress are taken into consideration, thus τ_{crit} is used to define the shear strength of masonry joints (t_s^{max} and t_t^{max}). Correspondingly, the possible pre-failure enhancement in shear behaviour due to frictional resistance is considered in the crack initiation criterion of masonry joints in the surface-based cohesive model.

In addition, the coefficient of friction of the masonry joints is defined to simulate the post-failure shear sliding behaviour (Tangential behaviour). The critical sliding shear stress ($\tau_{sliding}$) is obtained based on the friction law Eq. (6), which is governed by a linear relationship between the coefficient of friction and normal compressive stress.

$$\tau_{sliding} = \mu\sigma_n \tag{6}$$

The above friction formulation indicates the sliding of masonry units when the shear stress in the failed masonry joints is more than the critical sliding shear stress ($\tau_{sliding}$).

Once the damage initiation criterion is reached, the propagation of cracks in the masonry joints causes stiffness degradation at a defined rate which leads to total strength loss and failure of joints. Thus, Eq. (1) is rewritten as Eq. (7):

$$\boldsymbol{t} = (1 - D)\boldsymbol{K}\delta \tag{7}$$

D is the damage evolution variable, the value increases from 0 to 1 as per continuity of traction stresses after the damage initiation criterion met. In this study, a linear damage evolution variable is assumed by specifying the energy dissipated as a result of the damage process Fig. 3. The damage variable is expressed as:

$$D = \frac{\delta_{eff}^f(\delta_{eff}^{max} - \delta_{eff}^o)}{\delta_{eff}^{max}(\delta_{eff}^f - \delta_{eff}^o)} \tag{8}$$

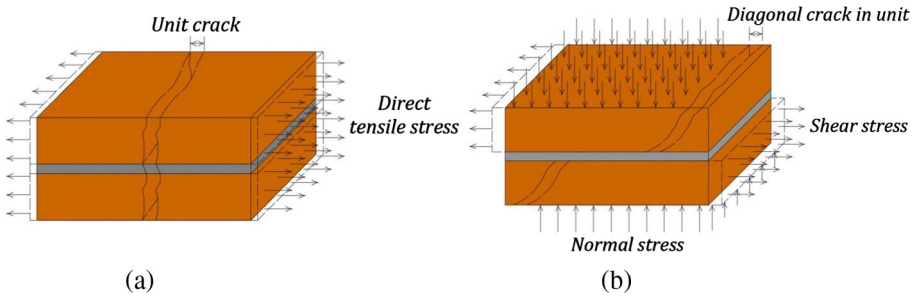

Fig. 4. Failure modes of the units: (a) direct tensile crack, (b) diagonal crack.

The effective separation δ_{eff}, is given by [19]:

$$\delta_{eff} = \sqrt{\langle \delta_n \rangle^2 + \delta_s^2 + \delta_t^2} \tag{9}$$

The effective separation at complete failure δ_{eff}^{f}, is also expressed as:

$$\delta_{eff}^{f} = \frac{2G_{TC}}{t_{eff}^{o}} \tag{10}$$

δ_{eff}^{f} is the effective separation at the complete failure of the joint, δ_{eff}^{0} is the relative effective separation when damage initiates in the joints, δ_{eff}^{max} is the maximum effective separation reached during the loading history. The critical mixed mode fracture energy, G_{TC}, is obtained from the Benzeggagh-Kenane (BK) law [20] since it is the most suitable when the critical fracture energies of both shear directions (mode II and mode III) are the same, which is the case in masonry joints. The exponent, η, in the BK law is set as 2 assuming brittle behaviour [20] in masonry joints. The critical fracture energy G^{C}, under the mixed-mode in the BK law is expressed as:

$$G_{TC} = G_{IC} + (G_{IIC} - G_{IC})\left\{\frac{G_{II} + G_{III}}{G_I + G_{II} + G_{III}}\right\}^{\eta} \tag{11}$$

2.2. Extended finite element method (XFEM)

The extended FEM approach (XFEM) was originally developed by Belytschko and Black [21] to simulate crack propagation in an element based on the nodal displacements of the element around the crack tip and without the requirement for re-meshing. In the XFEM, discontinuous enrichment functions are added to the classical FEM based on the partition of unity concept proposed by Melenk and Babuska [22]. The enrichment functions, which make the crack independent of the mesh, are expressed as the approximation for a displacement vector function, $\boldsymbol{u}$, and is written as below [23]:

$$\boldsymbol{u} = \sum_{I \in N} N_I(x)\left[u_I + H(x)a_I + \sum_{\propto=1}^{4} F_{\propto}(x) b_I^{\propto}\right] \tag{12}$$

In the above enrichment functions, $N_I(x)$ is associated with nodal shape functions, u_I is nodal displacement vector, $H(x)$ is associated with discontinuous jump functions to form the crack path, a_I is vector of the nodal enriched degree of freedom, $F_{\propto}(x)$ is associated with the crack-tip functions to develop cracks at the tip and $b_I^{\propto}$ is the vector of the nodal enriched degree of freedom.

In this paper XFEM is used to simulate crack initiation and propagation in masonry units under tension and shear Fig. 4 without *a priori*-specification of a crack path and crack location. XFEM cracks are simulated based on the cohesive segment method [24]. The method can follow the traction separation law described above for the surface based cohesive behaviour to initiate and propagate cracks in the elements of masonry units.

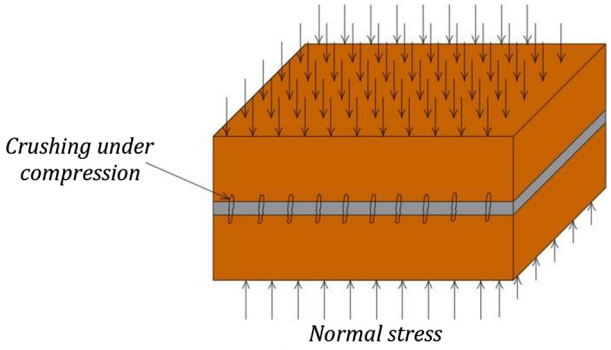

Fig. 5. Crushing of masonry assemblage under compression.

2.3. Drucker-Prager plasticity model

The Drucker-Prager plasticity model is used to simulate the compressive non-linear behaviour of masonry. The model allows the isotropic hardening and softening of materials under compression. Thus, the possible compressive failure of masonry can be captured Fig. 5.

The DP model was originally developed by Drucker and Prager [25] as a generalisation of the Mohr-Coulomb criterion to estimate failure stress of frictional materials such as soils and rocks. The model was then modified by Lubarda et al. [26] to include the compressive yield criterion under hydrostatic compaction pressure. In this paper, a linear yield criterion is adopted, which is a linear yield surface in the meridional (p–t) plane Fig. 6. The evolution of the yield surface with non-linear deformation was defined based on the uniaxial compression yield stress, σ_c, of the masonry assemblage. In this criterion, flow stress ratio R, dilation angle ψ, and friction angle β, are to be defined. The linear yield surface in the DP plasticity model is expressed as [27]:

$$F = t - p\tan\beta - d = 0 \tag{13}$$

where

$$t = \frac{1}{2}q\left[1 + \frac{1}{R} - \left(1 - \frac{1}{R}\right)\left(\frac{r}{q}\right)^3\right] \tag{14}$$

The hydrostatic pressure stress, p, is given by:

$$p = -\frac{1}{3}trace(\boldsymbol{\sigma}) \tag{15}$$

And the von Mises equivalent stress, q, is given by:

$$= \sqrt{\frac{3}{2}(\mathbf{S} : \mathbf{S})} \tag{16}$$

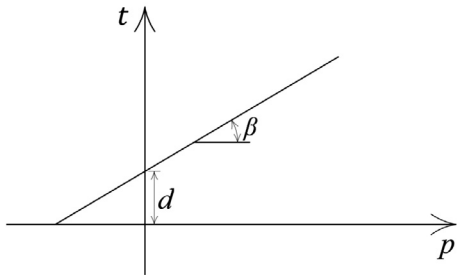

Fig. 6. Linear yield surface of the DP model (based on [27]).

$$\mathbf{S} = \sigma + p\mathbf{I} \tag{17}$$

$$r = \left(\frac{9}{2}\mathbf{S}\cdot\mathbf{S}:\mathbf{S}\right)^{\frac{1}{3}} \tag{18}$$

$$d = \left(1 - \frac{1}{3}\tan\beta\right)\sigma_c \tag{19}$$

The compressive plastic properties of a masonry system i.e. the values of compressive yield stresses versus absolute plastic strains are defined as the hardening and softening behaviour of the DP plasticity model via the expanded masonry units, thus the compressive yield surface of masonry was included in the FE models.

2.4. Elastic behaviour of expanded units

The elastic modulus of the expanded masonry units must be adjusted and made to have an equivalent elastic response to the original masonry assemblage (unit and mortar). It is to be determined by taking the original masonry unit and mortar moduli of elasticity and geometry of the masonry assemblage into account. For this purpose, Eq. (20) is proposed based on the assumption of a stack bond between masonry units and uniform stress distribution in masonry constituents. It is presented as:

$$E_{adj} = \frac{HE_uE_m}{nh_uE_m + (n-1)h_mE_u} \tag{20}$$

3. Finite element modelling and analysis

In the proposed 3D finite element simplified Micro-model, the linear and non-linear behaviour of expanded units and interfaces are defined. The expanded units are modelled using 3D hexahedral shaped eight node linear brick elements with reduced integration and hour glass control (type C3D8R) [27]. The joint interfaces are modelled based on a surface based cohesive approach. The contacts between adjacent masonry units are defined through a node to surface discretisation method with finite sliding formulation. Hard contact behaviour was defined between the adjacent surfaces of masonry units by the contact pressure-overclosure relationship. The adopted hard contact behaviour assumes that the surfaces transmit pressure when they are in contact. In addition, the penetration and the transfer of tensile stress between the contacting surfaces are prevented in the hard contact model. This model corresponds with the behaviour of the contacting surfaces of masonry units.

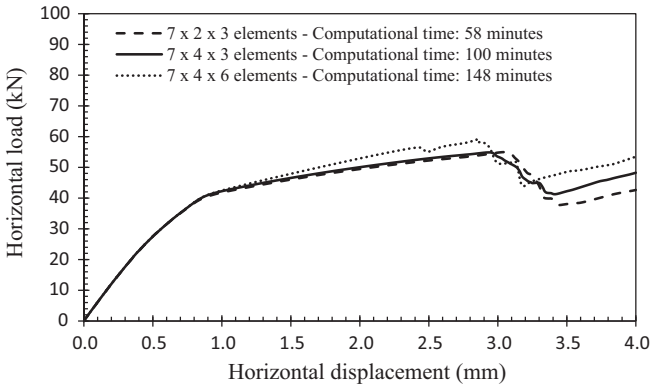

Fig. 8. Horizontal load-displacement response with different mesh sizes.

The simplified Micro-models presented in this study are generated in Abaqus/Standard. The mesh generation of the models is conducted via a simple piece of code, in this case Python script; this code significantly reduces the time and effort required for generating simplified Micro-models. The mesh size was chosen based on a mesh sensitivity study. For this purpose, three numerical analyses were conducted for the masonry wall which is represented later for the validation study under in-plane loads. In the first analysis, each masonry unit (210 mm long × 52 mm high × 100 mm thick) was modelled with 7 × 2 × 3 elements Fig. 7(a). In the second, each unit was modelled with 7 × 4 × 3 elements Fig. 7(b), double the number of elements compared to the first case. In third analysis, each unit was modelled with 7 × 4 × 6 elements Fig. 7(c), i.e. 4 times the number of elements used in the first case. In all cases, the results in terms of failure patterns, and elastic and plastic response were satisfactorily similar as shown in Fig. 8. This comparison indicates the relative insensitivity of the proposed model to the given mesh sizes. In turn, relatively course meshes can be used which significantly reduces the required computational time.

The steps adopted to conduct the numerical analysis impose the actions (load or displacement) to the model either based on load control or displacement control. In both cases, the actions are incrementally imposed. Large displacement non-linear geometry effects were considered in all models. A general non-linear static procedure was adopted to follow a Newton-Raphson algorithm solution which iteratively solves for equilibrium in each increment. In addition, stiffness degradation and softening behaviour of masonry joints induce numerical instability; therefore viscous regularisation is required as a damage stabiliser in the surface-based cohesive

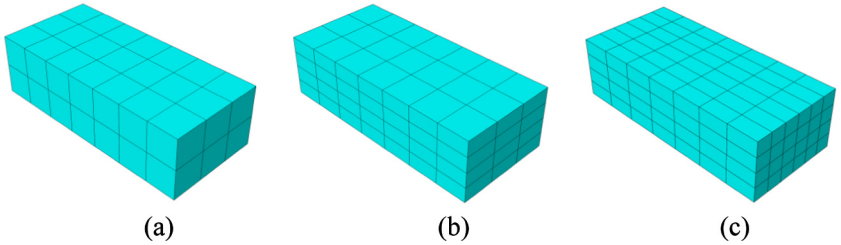

Fig. 7. Masonry units with different mesh sizes.

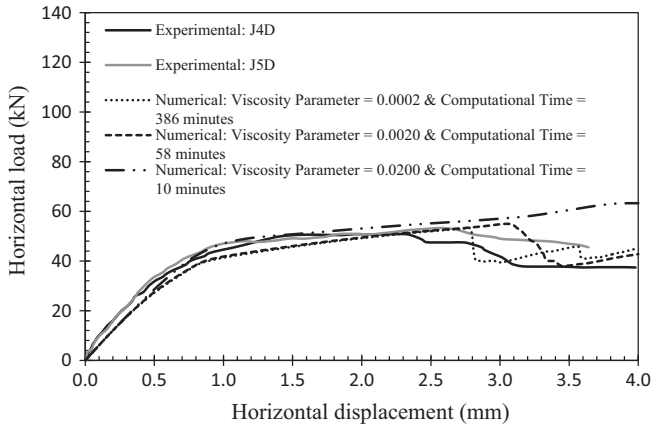

Fig. 9. Comparison between horizontal load-displacement responses and computational times using different viscosity parameters.

behaviour model to simulate the full failure of masonry joints without numerical convergence difficulties. To obtain an appropriate viscosity parameter for specifying the stabilisation in masonry joints, parametric studies were conducted. In this parametric study, the viscosity parameter was adopted by considering the computational time, the effect of the parameter on the overall response of the model and the convergence of numerical analysis. For this purpose, three different viscosity parameters were tested by simulating the wall used as the validation example under in-plane load; while mesh size was kept constant (each masonry unit was modelled with $7 \times 2 \times 3$ elements Fig. 7(a)). The detailed comparison between numerical results using different viscosity parameters are shown in Fig. 9. Based on this study and by considering a balance between the accuracy of results and computational time, the viscosity parameter was adopted as 0.002 for the rest of the numerical analyses.

4. Validation examples

The capability of the proposed 3D combined simplified Micro-model to simulate the structural behaviour and various failure mechanisms of masonry is presented. For this purpose, simulations of a number of masonry panels from three different experiments are conducted under different loading conditions, namely, monotonic in-plane, out of plane and in-plane cyclic loads. The numerical results are then compared to those obtained from the corresponding experiments.

4.1. Response of masonry under in-plane loading

The data and results of experimentally tested masonry shear walls undertaken and reported in [28] are adopted to validate the numerical model under in-plane loading. The dimensions of the tested shear walls were 900 mm long × 1000 mm high × 100 mm thick. Each wall was built with 18 courses of wire cut solid clay bricks, the brick dimensions were 210 mm long × 52 mm high × 100 mm thick. The thickness of the mortar joint was 10 mm and was made of cement, lime and sand with a volumetric ratio of 1:2:9 respectively. Both the top and bottom courses of the walls were clamped via steel beams, the bottom beam being fixed to the lab floor. The walls were subjected to an imposed vertical compressive stress via the top beam. After applying the compressive load, the vertical movement of the top beam was restrained, and then a monotonic load was horizontally applied to the walls via the top beam Fig. 10.

In the experiment, masonry shear walls under different imposed vertical compressive stresses were tested. The failure modes of the walls were due to a combination of diagonal cracks and cracking of units themselves, followed by crushing under compression. In the present study three walls with two different initial compressive stresses were considered, namely, wall J4D and J5D under 0.3 MPa and wall J6D under 1.21 MPa. These values were chosen based on the values of the imposed compressive stresses reported in the corresponding experiments [28]. The mechanical properties and data used for defining the numerical models were obtained from the experimental results reported in [28], the data used in [4] and using Eqs. (2) and (20). The mortar elastic modulus (E_m) was calculated by considering the given values of K_{nn} and E_u and using Eq. (2). Then, the adjusted elastic modulus (E_{adj}) of the

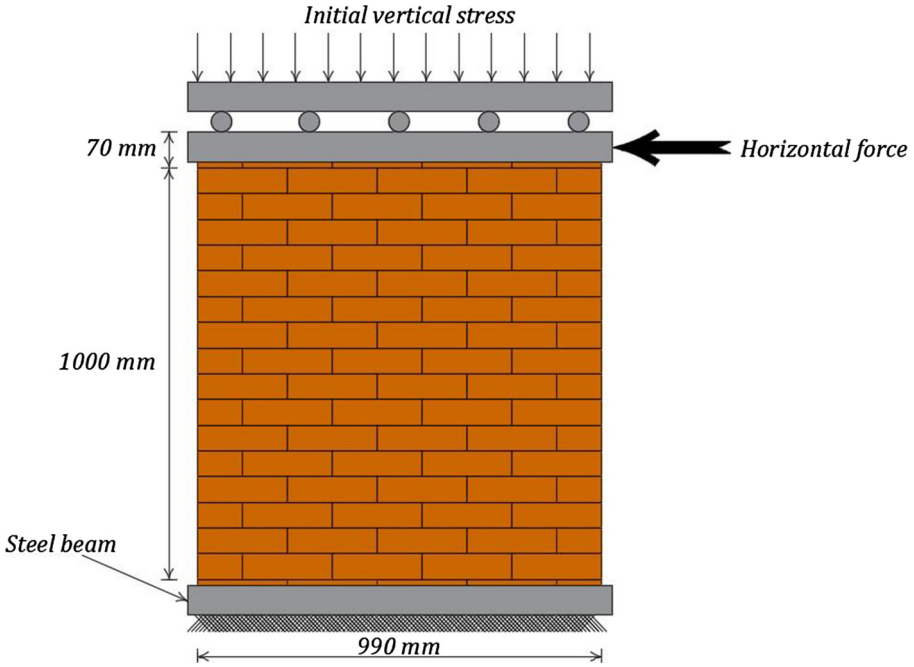

Fig. 10. Test set up of masonry shear walls (based on [28]).

Table 1
Elastic properties of constitutive materials and joint interfaces for the wall tested under in-plane load.

Wall	Brick units		Mortar	Expanded units	Joint interface		
	E_u (MPa)	v	E_m (MPa) (from Eq. (2))	E_{adj} (MPa) (from Eq. (20))	K_{nn} (N/mm^3)	K_{ss} (N/mm^3)	K_{tt} (N/mm^3)
J4D and J5D	16,700	0.15	780	4050	82	36	36
J6D	16,700	0.15	1030	4655	110	50	50

Table 2
Non-linear material properties for the joint interfaces.

Wall	Tension			Shear		Compression
	t_n^{max} (MPa)	G_{IC} (N/mm)	c (MPa)	μ	G_{IIC} (N/mm)	σ_c (MPa)
J4D and J5D	0.25	0.018	0.350	0.75	0.125	10.5
J6D	0.16	0.012	0.224	0.75	0.050	11.5

Table 3
Properties for the masonry units for the wall tested under in-plane load.

Tension		Shear	
Tensile strength (MPa)	G_{IC} (N/mm)	Shear strength (MPa)	G_{IIC} (N/mm)
2.0	0.08	2.8	0.50

masonry wall was calculated using Eq. (20). All parameters used in this validation study are summarised in Tables 1–3.

As discussed earlier, crushing of the masonry under compression is simulated in the expanded masonry units by using the Drucker Prager model. To do so, the hardening and softening parts of axial compressive stresses versus plastic strain of the masonry assemblages are required. In addition, other required parameters such as dilation angle (ψ), friction angles (β) and flow stress ratio (R) are defined as follows; ψ was selected as a lower bound as 11.3 degrees based on [29], β is set at 36 degrees based on the coefficient of friction for masonry units and K was set as the default value equal to 1 [27]. The compressive stress-strain curves required to define the compressive behaviour of the numerical models were obtained by considering the study conducted by Kaushik et al. [30], making use of the ultimate compressive strength values (σ_c) given in the experiments and the adjusted elastic modulus value (E_{adj}) calculated from Eq. (20). For detailed information, the reader is referred to [30]. The compressive stress strain curves are shown in Fig. 11(a) and (b).

For the simulation, 3D eight node linear brick elements were used, the longest side of the elements was 30 ∓ 3 mm which resulted in a mesh comprising 3456 elements as shown in Fig. 12. The numerical analysis was computed in two steps. In the first step, the initial vertical compression stress was imposed. To keep the same boundary conditions as in the experiment, in the second step, the vertical and out of plane horizontal displacements and rotations about all axes were restrained at the top of the wall, and the horizontal in-plane monotonic load was incrementally applied under displacement control, with the imposed vertical compression stress held constant.

The numerical results show a good agreement with experimental results in terms of load displacement relationships Fig. 13. Furthermore, the failure modes of the numerical models were consistent with the experiments. For example in the J4D and J5D walls, the mode of failure in both experiments Fig. 14(a) and numerical models Fig. 14(b) were characterised by initiation of tensile cracks at the top and bottom of the wall at an early loading stage Fig. 15(a). These cracks were then followed by formation of diagonal stepped cracks between masonry units, cracking of the masonry units themselves and eventually crushing of the top and bottom toes under compression which ultimately led to failure of the walls Fig. 15(b).

The term STATUSXFEM in Fig. 14(b) indicates the cracking status of the elements; the value of 1 signifies complete cracking of the element, 0 indicates no cracking, and values between 0 and 1 indicate partial cracking of the elements. A good agreement between the distributions of cracked units can also be observed in the experimental and numerical walls.

Fig. 15(a) shows cracks at the top and bottom of the wall and the compressive stresses are distributed over the undamaged regions of the wall. In Fig. 15(b), the cracks propagated along the head and bed joints, and in the masonry units themselves. These cracks resulted in the redistribution of compressive stresses over

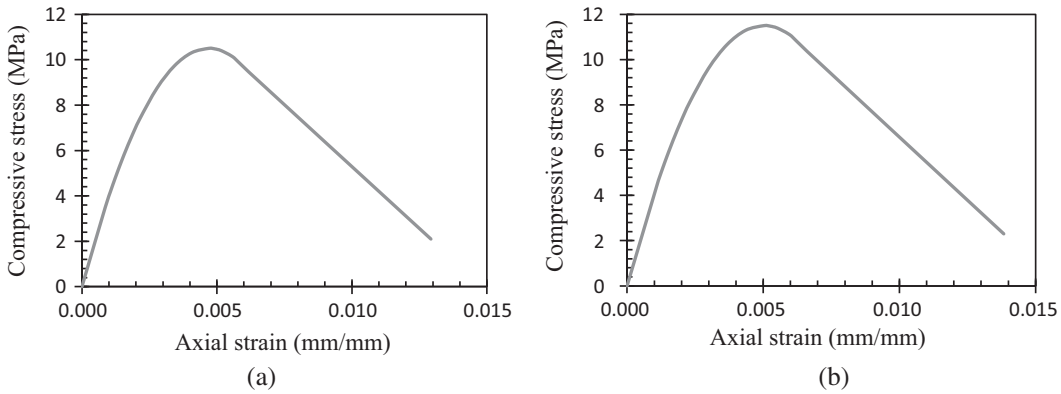

Fig. 11. Compressive stress-strain curves: (a) J4D and J5D walls; (b) J6D.

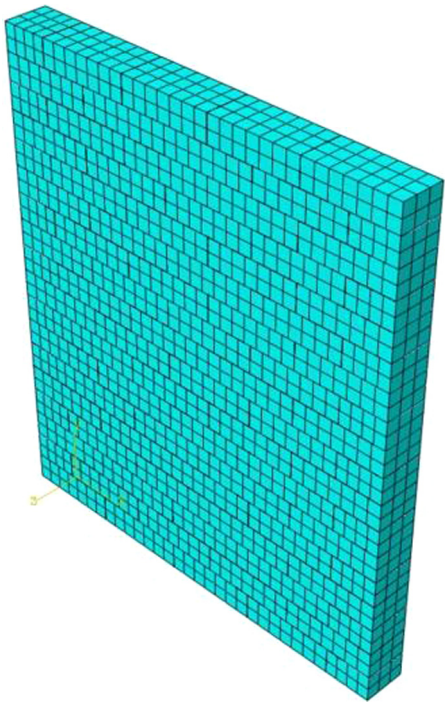

Fig. 12. Generated mesh of numerical models.

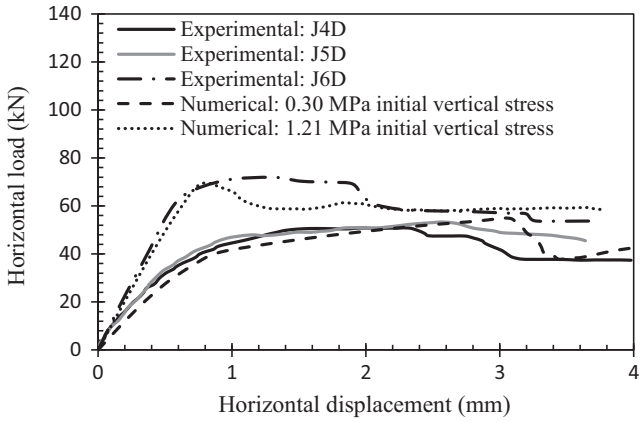

Fig. 13. Comparison between experimental and numerical results.

the un-cracked regions and occurrence of high compressive stresses and crushing of the wall at its toe.

4.2. Response of masonry under out-of-plane loading

The focus of this validation study is the on-plan C-shaped masonry wall tested by Griffith and Vaculik [31] under out of plane loading, see Fig. 16. The main portion of the wall forming the web was 4 m long and 2.5 m high, the return walls which formed the flanges were 0.45 m long and 2.5 m high, in all cases the wall was 110 mm thick. The wall was built with 10-hole cored 230 mm long × 76 mm high × 110 mm thick brick units with a mortar joint thickness of 10 mm (1:2:9 cement:lime:sand), the bond pattern was half overlap stretcher bond. The wall was simply supported along its entire length at the top and bottom. The return walls were built along the vertical edges of the main wall (web) to provide a realistic moment restraint and the free ends of the return walls were clamped by a steel channel section which restrained the lateral movements Fig. 16. The wall was loaded by applying pressure to the outer face of the web wall via an airbag placed between the web and a reaction frame. The recorded forces in the reaction frame were then divided by the surface area of the web to determine the applied pressure. The response of the wall was presented as a relationship between the applied pressure and out of plane displacement at the centre of the inner surface of the main web.

The material properties required for defining the numerical model were obtained from the original experimental data. Where properties were not reported in the experiments, these were obtained either by calculation or assumptions based on relevant data available in the literature detailed as follows. Poisson's ratio was set as 0.15, similar to the previous validation study as reported in [28]. The mortar elastic modulus (E_m) was calculated based on the given values of brick units (E_u) and masonry (E_{adj}) elastic

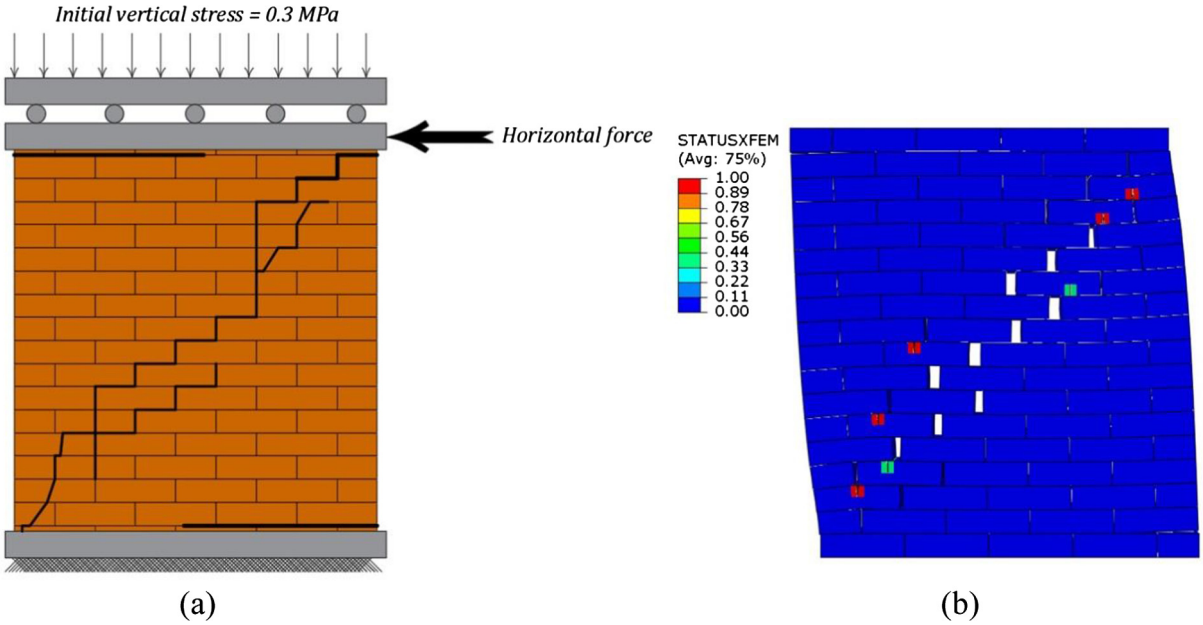

Fig. 14. Comparison of failure modes: (a) experimental failure patterns; (b) numerical failure patterns (scale factor = 20).

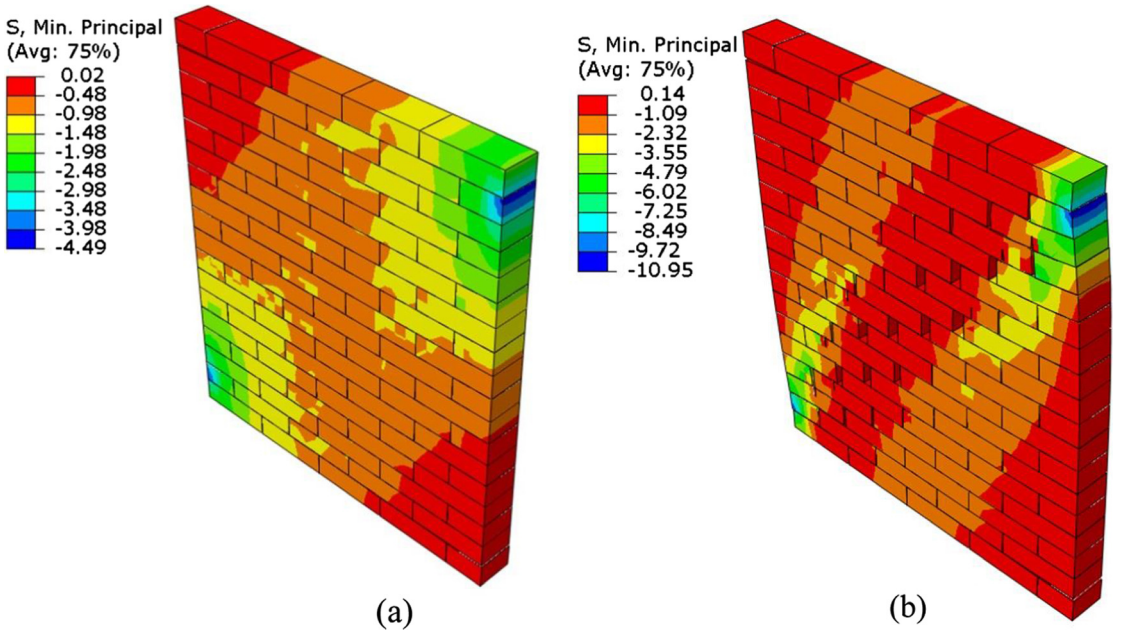

Fig. 15. Crack pattern and minimum principal stress distribution (N/mm^2) in the wall with the initial vertical compression stress of 0.3 N/mm^2: (a) at 1 mm horizontal displacement at top; (b) at 4 mm horizontal displacement at top (scale factor = 20).

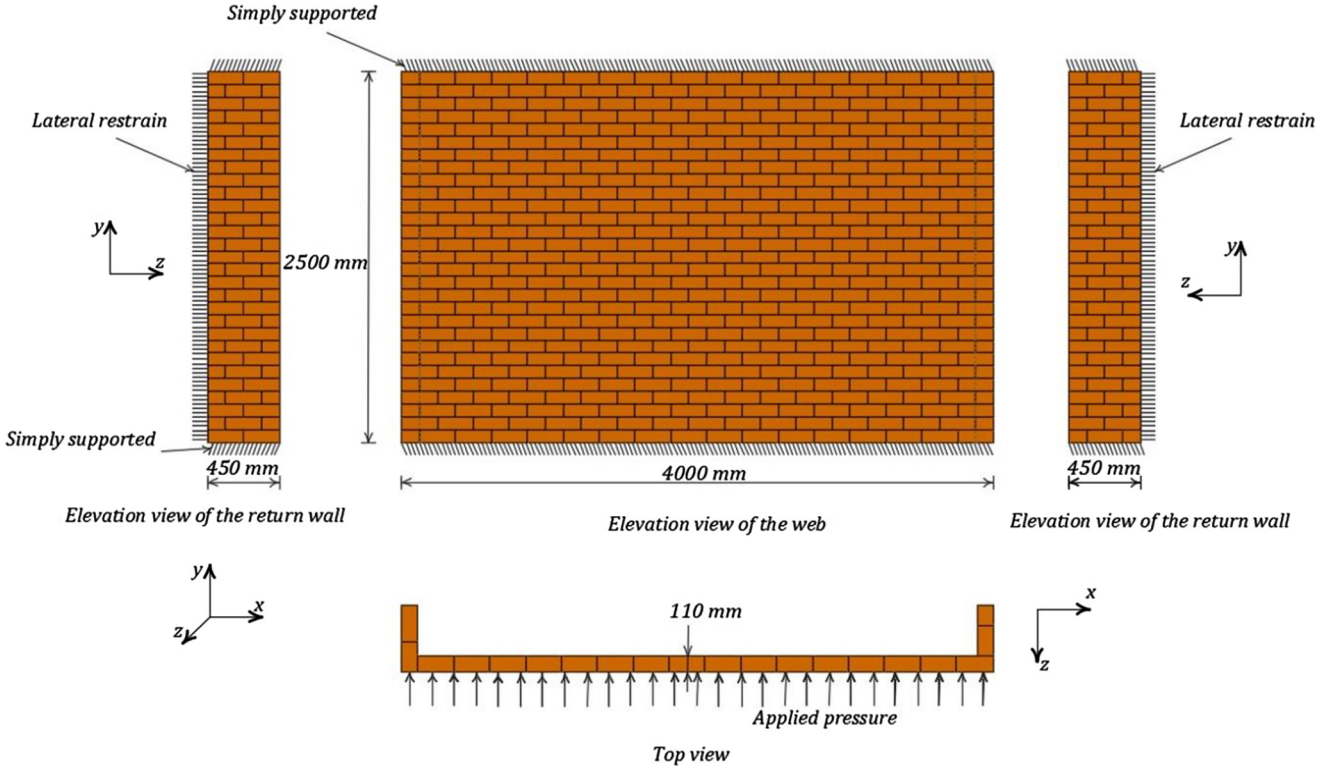

Fig. 16. Wall configuration (based on [31]).

moduli reported in [31] and using Eq. (20). The elastic stiffness of joint interfaces in the normal and shear directions (K_{nn}, K_{ss} and K_{tt}) were calculated by using Eqs. (2) and (3). The values of G_u and G_m in Eqs. (2) and (3) are considered as 0.4 of E_u and E_m respectively, as recommended in Eurocode 6 [32]. The tensile bond strength of joints (t_n^{max}) was considered as one third of the flexural strength (f_{mt}) of the masonry system as recommended in [33]. The flexural strength of the masonry system was calculated based on the virtual work method by considering the experimental results reported in [31] i.e. the ultimate horizontal load carrying capacity (3.04 kPa), the collapse mechanism (yield line) was idealised from the experimental result as shown in Fig. 17. In addition, the

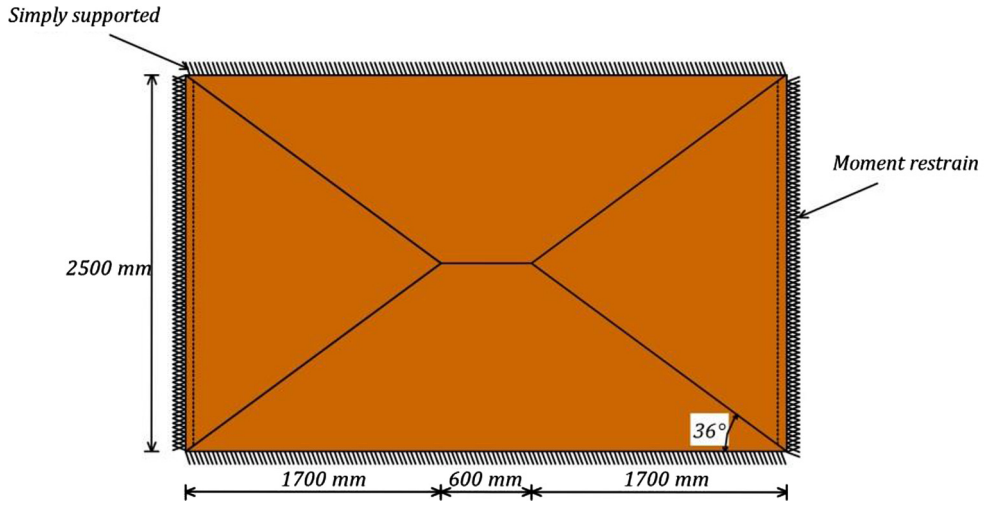

Fig. 17. The idealised failure mechanism considered in the virtual work method.

Table 4
Elastic properties of constitutive materials and joint interfaces for the wall tested under out of plane load.

Brick units		Mortar	Expanded units	Joint interface		
E_u (MPa) [31]	v [28]	E_m (MPa) (from Eq. (20))	E_{adj} (MPa) [31]	K_{nn} (N/mm^3) (From Eq. (2))	K_{ss} (N/mm^3) (From Eq. (3))	K_{tt} (N/mm^3) (From Eq. (3))
52,700	0.15	420	3540	42	17	17

Table 5
Non-linear material properties for the joint interface for the wall tested under out of plane load.

Tension		Shear			Compression
t_n^{max} (MPa) (Calculated)	G_{IC} (N/mm) [36]	c (MPa) (Calculated)	μ, [28]	G_{IIC} (N/mm) (assumed based on [4])	σ_c (MPa) [31]
0.12	0.012	0.17	0.75	0.040	16

horizontal (M_h) and diagonal (M_d) bending moment capacities for the case shown in Fig. 17 were determined by using Eqs. (21) and (22) reported in [34,35], respectively.

$$M_h = \frac{1}{(h_u + h_m)}\left[\tau_{crit} k_b 0.5 (l_u + h_m) t_u^2\right] \tag{21}$$

$$M_d = \frac{\sin \varnothing}{(h_u + h_m)}\left[(\sin \varnothing)^3 \tau_{crit} k_b 0.5 (l_u + h_m) t_u^2 + (\cos \varnothing)^3 f_{mt} \frac{0.5 (l_u + h_m) t_u^2}{6}\right] \tag{22}$$

In the above equations, k_b is a numerical factor and taken as 0.214 for stretcher bond masonry walls, and $\varnothing$ the angle of the diagonal crack line.

The value of tensile fracture energy is not dependant on the tensile bond strength of joints, the average value of 0.012 N/mm is recommended in the absence of detailed information by Angelillo et al. [36]. The cohesion value of the joint interfaces was considered as 1.4 of the tensile bond strength as implemented in [4]. The shear fracture energy of masonry joints was set at 0.04 N/mm. According to [4], the shear fracture energy of masonry joints with a cohesion strength (c) ranging from 0.1 to 1.8 MPa ranges from 0.01 to 0.25 N/mm. In this study, 0.04 N/mm was adopted with a view of giving best agreement between experimental and numerical results. In Table 6, the tensile strength of the units was considered as one third of the flexural strength of the units reported in the experiments. The shear strength of the units was set as 1.4 of their tensile strength. The tensile and shear fracture energies were considered to be the same as the fracture energies used in Table 3, assuming similar fracture behaviour of masonry units. The material parameters used for the numerical model under out-of-plane loading are summarised in Tables 4–6.

Table 6
Properties for the masonry units for the walls tested under out of plane and cyclic loads.

Tension		Shear	
Tensile strength (MPa) (from flexural strength [31])	G_{IC} (N/mm) [28]	Shear strength (MPa) (1.4 of tensile strength)	G_{IIC} (N/mm) [28]
1.18	0.08	1.65	0.50

Similarly above, the dilation angle (ψ), friction angles (β) and flow stress ratio (R) are defined as 11.3 degrees, 36 degrees and 1, respectively, for the Drucker Prager model. The compressive stress strain curve was obtained Fig. 18 based on [30], making use of the ultimate compressive strength value (σ_c) and masonry elastic modulus (E_{adj}) given in the experiment [31].

The wall model consisted of 11252 3D eight node linear brick elements; the side length of each element was 50 ∓ 10 mm. The analysis was conducted in one step, with the out of plane pressure imposed to the outer surface of the main wall under load control. The computational time required to conduct the analysis was 238 min (PC specification: 16 GB RAM, Intel i7 Core Processor with 3.4 GHz clock rate).

The numerical surface pressure versus displacement response of the wall showed a good agreement with the experimental

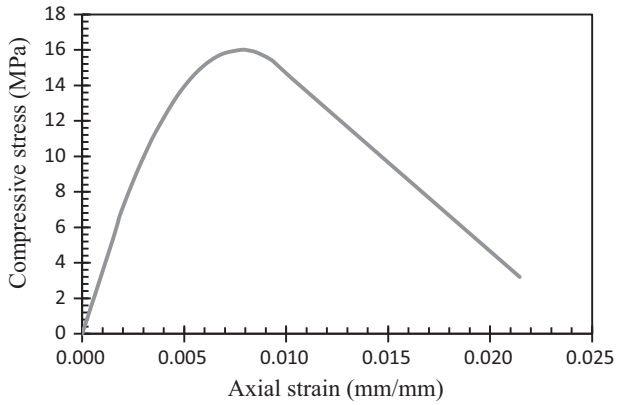

Fig. 18. Compressive stress-strain curve of the masonry system.

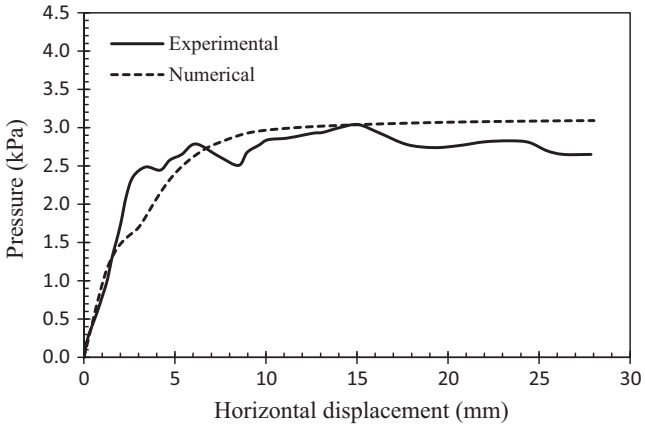

Fig. 19. Relationship between applied pressure and deflection at the centre of the main wall inner face: experimental and numerical.

response. It was reported in the experiment that, the post peak strength response of the wall was relatively constant from the beginning of non-linear behaviour until reaching excessive displacement. This response was reported as being due to redistribution; initially mobilising the diagonal bending moment resistance via stepped diagonal cracks, then the horizontal bending moment resistance provided by the vertical edges of the return walls. The same response was captured in the numerical model Fig. 19.

The experimental mode of failure in [31] is reported as the formation of horizontal cracks at mid height of the inner wall and stepped diagonal cracks extending from the middle to the corners at the inner surface of the main wall Fig. 20(a). This scenario was also well captured in the numerical model Fig. 20(b). At this stage in the experiment, the wall was unloaded and no further damage in the wall was reported in [31], similarly at the same loading stage the numerical model showed no complete cracks in the actual masonry units themselves, or crushing of masonry of under compression Fig. 21, and the numerical model continued to sustain further pressure. However, the numerical model shows multiple distributed diagonal cracks rather than individual diagonal cracks as occurred in the experiment. This difference may be due to the inaccuracies in the adopted material properties. As previously discussed, some of the material parameters used in the numerical model have been estimated based on relevant parameters available in the literature, this situation is due to the absence of all required parameters in the experiment. Another potential source of difference is the fact that the properties of the unit-mortar interfaces were defined to be the same in the entire wall, this assumption results in the equal contribution of the unit-mortar joints to distribute the flexural stresses in the regions of the concentrated stresses. Realistically, the strength of the unit-mortar joints is unlikely to be entirely uniform within a masonry assemblage due to various effects such as workmanship, quality of mortar, etc. Correspondingly, the cracks usually form individually along the relatively weaker joints.

Fig. 22 shows the cracking status in masonry units at the final loading stage. Similar to the experimental results, no complete cracking of masonry units was observed in the numerical results. The STATUSXFEM shows the masonry units with partial cracks, which indicates the potential cracks in vulnerable masonry units at the corners of the main wall outer face due to high tensile stresses.

4.3. Response of masonry under in-plane cyclic loading

The experimental results reported in [37] are used to validate the proposed model against the masonry behaviour under static in-plane cyclic loads. The nominal dimensions of the tested walls reported in [37] were 1200 mm long × 1200 mm high × 110 mm thick. The walls were built using 10-hole clay bricks with dimensions of 230 mm long × 76 mm high × 110 mm thick with a mortar joint thickness of 10 mm (1:1:6 cement:lime:sand). Each wall had 5 bricks in a row and 14 courses of brick, which were put in a running bond. A series of walls were tested to investigate the behaviour of masonry when a damp-proof course (DPC) is placed either in the first bed joint or between the bottom of the wall and its supporting base. The walls were placed on a concrete beam which was attached to a steel spreader beam which was in turn fixed to the floor; the vertical and horizontal loads were imposed

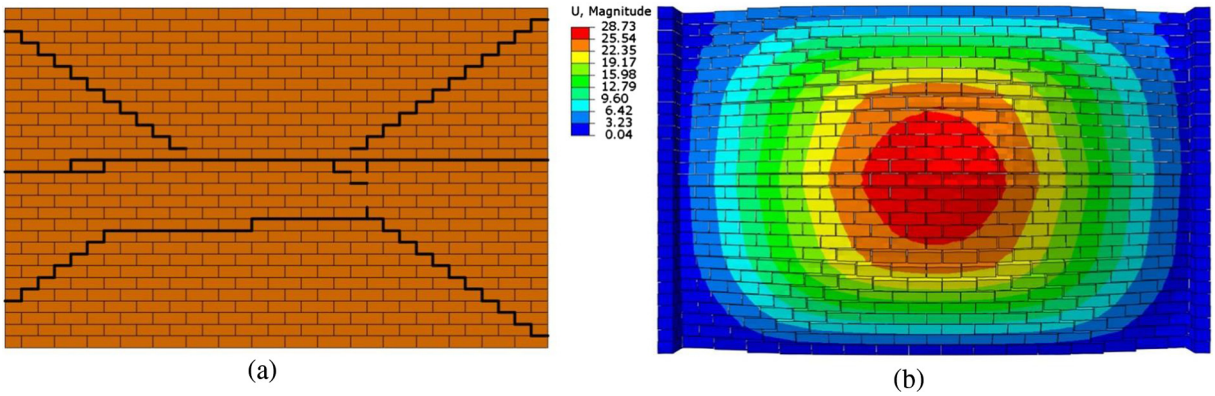

Fig. 20. Comparison between failure mode patterns: (a) experimental; (b) numerical with scaling factor 20.

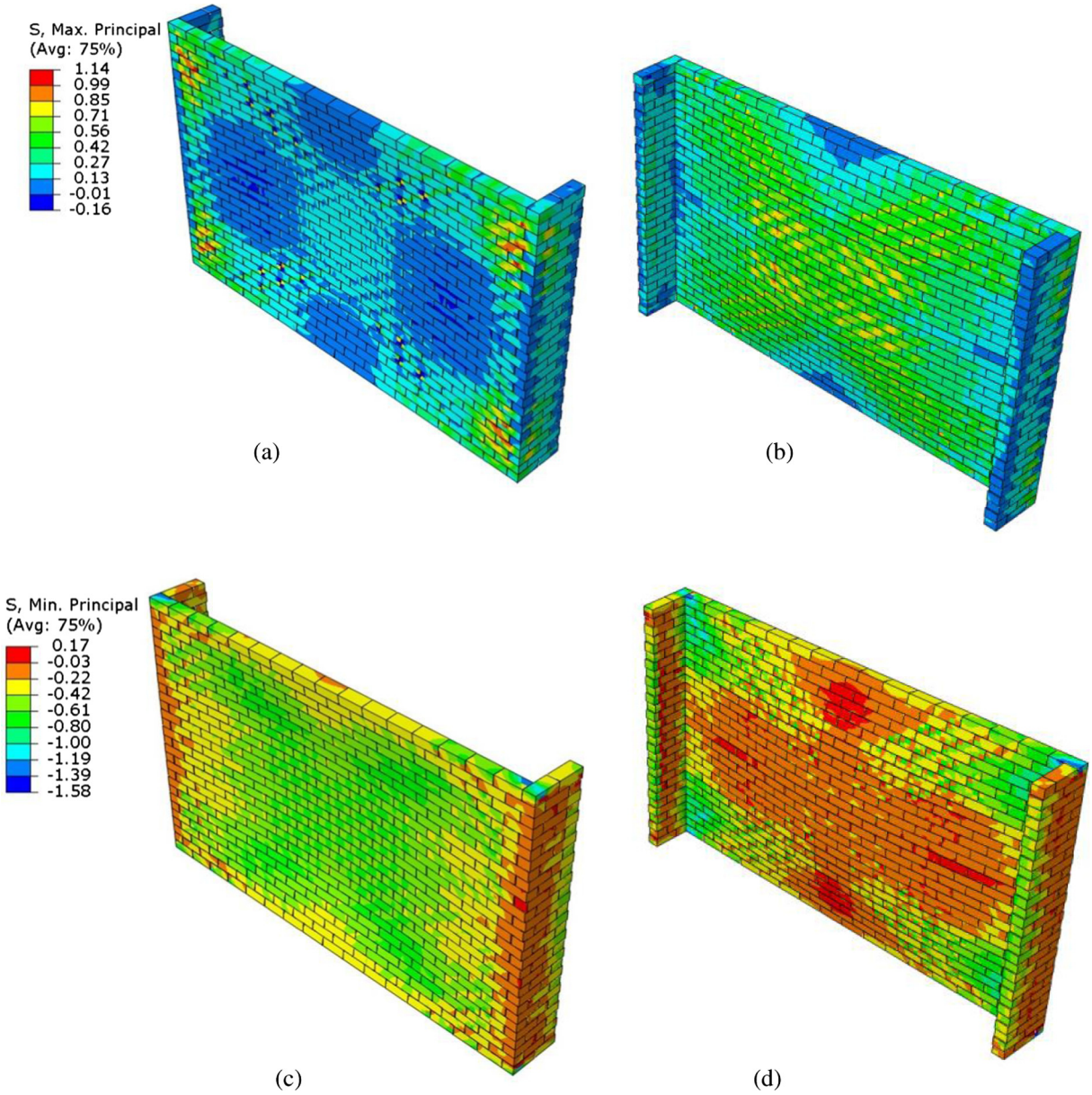

Fig. 21. Stress distributions in the walls at 28.73 mm deflection at the centre of the web (N/mm^2): (a) and (b) Tensile stresses; (c) and (d) Compressive stresses.

to the top of the walls via a spreader beam Fig. 23. The loads were applied in two steps, initially a pre-compression vertical stress was applied which was kept constant during the tests, and then the walls were subjected to horizontal in-plane cyclic loads under displacement control. The wall considered for this study was subjected to 19 number of cycles, Fig. 24 shows the load protocols applied to the top of the wall. For this study, a wall, which has been subjected to an initial vertical stress of 0.7 MPa, is considered. The wall is labelled as A3-1 in the experiments, in which a DPC layer has been placed in the bed joint between first and second course.

The mechanical properties used in the numerical models were obtained either from the experimental results reported in [37] or calculated or assumed based on the relevant data available in the literature. The brick (E_u) and mortar (E_m) elastic moduli were calculated based on their compressive strength values reported in the experiments, E_u was set as 300 times the brick compressive strength and E_m was set as 100 times the mortar compressive strength based on the relations provided in [30]. The Poisson's ratio was assumed as 0.15 similar to the previous validation studies. Masonry elastic modulus (E_{adj}) was calculated by using Eq. (20). The elastic stiffness of joint interfaces in the normal and shear directions (K_{nn}, K_{ss} and K_{tt}) were calculated by using Eqs. (2) and (3). The tensile bond strength of joints (t_n^{max}) was calculated based on the flexural bond strength (f_{mt}) value reported in the experiments, t_n^{max} was considered as one third of f_{mt} as recommended in [33]. Similar to Table 5, the tensile fracture energy of the joint interfaces was set as 0.012 N/mm as recommended in [36]. The cohesion value of the joint interface was set as 0.64 MPa as reported in the experiment [37]. The shear fracture energy was considered as 0.04 N/mm, which was within the range of values recommended in [4]. The coefficient of friction was assumed as 0.75 similar to the previous validation studies. The mechanical properties of the units were assigned to be the same as the properties presented in Table 6, assuming the same behaviour, as the units in both cases were Australian 10-hole clay bricks with the same dimensions. In the bed joint, where the DPC layer was laid,

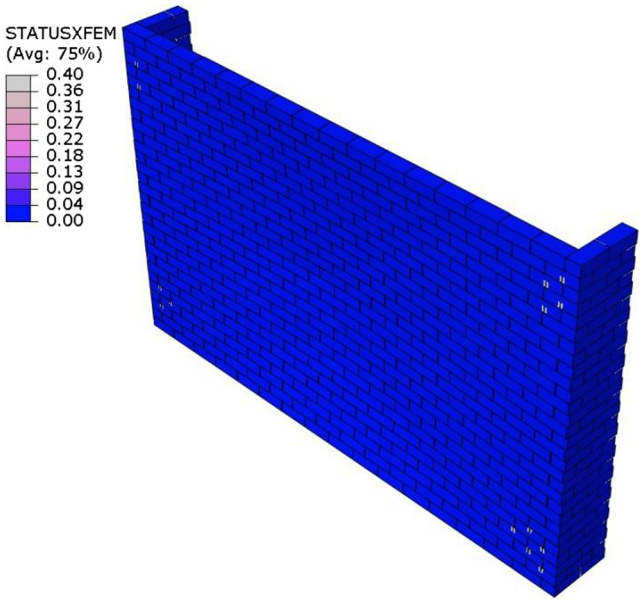

Fig. 22. Cracking status of masonry units (Partial cracking) at final loading stage, 28.73 mm deflection at the centre of the main wall.

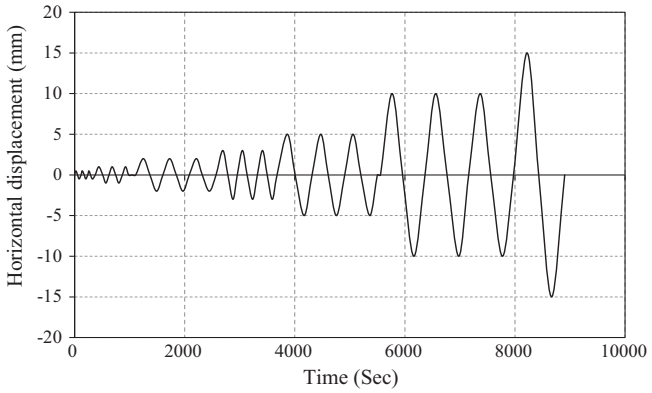

Fig. 24. In-plane horizontal displacement-time history (based on [37]).

the mechanical properties were defined as follows; the coefficient of friction and the cohesion were set as 0.425 and 0.038 MPa, respectively, as reported in the experiments [37]. The ratio of 1.4 as the cohesion value to the tensile bond strength value was considered to define the tensile bond strength as implemented in [4]. The tensile and shear fracture energies were calibrated as 0.001 N/mm and 0.0038 N/mm, respectively. All mechanical properties are summarised in Tables 7–9.

The dilation angle (ψ), friction angles (β) and flow stress ratio (R) are defined as 11.3 degrees, 36 degrees and 1, respectively, for the Drucker Prager model. The compressive stress-strain curve Fig. 25 was obtained based on [30] using the given value of the compressive strength in the experiments and calculated masonry elastic modulus (E_{adj}).

3D eight node linear hexahedral brick elements were used to model the masonry wall, the side of each element was 30 ∓ 3 mm, and the total number of elements in the mesh was 6720. The analysis was conducted in two steps. The initial vertical stress was applied to the top of the walls via a rigid body in the first step under load control. The rigid body was defined to simulate the top steel beam used in the experiments to distribute the stresses. In the second step, the cyclic in-plane load was subjected to the wall under displacement control via the rigid body, while the out of plane displacement and rotation were restrained. In addition, the initial vertical stress applied in the first step was kept constant. The computational time required was 552 min.

The numerical results show a good agreement with the experimental results for both horizontal force-displacement relationship and failure modes. The experimental and numerical force-displacement patterns sufficiently match in terms of initial stiffness and non-linear behaviour. The non-linear behaviour of the wall was quasi ductile due the energy dissipated by the bed joint

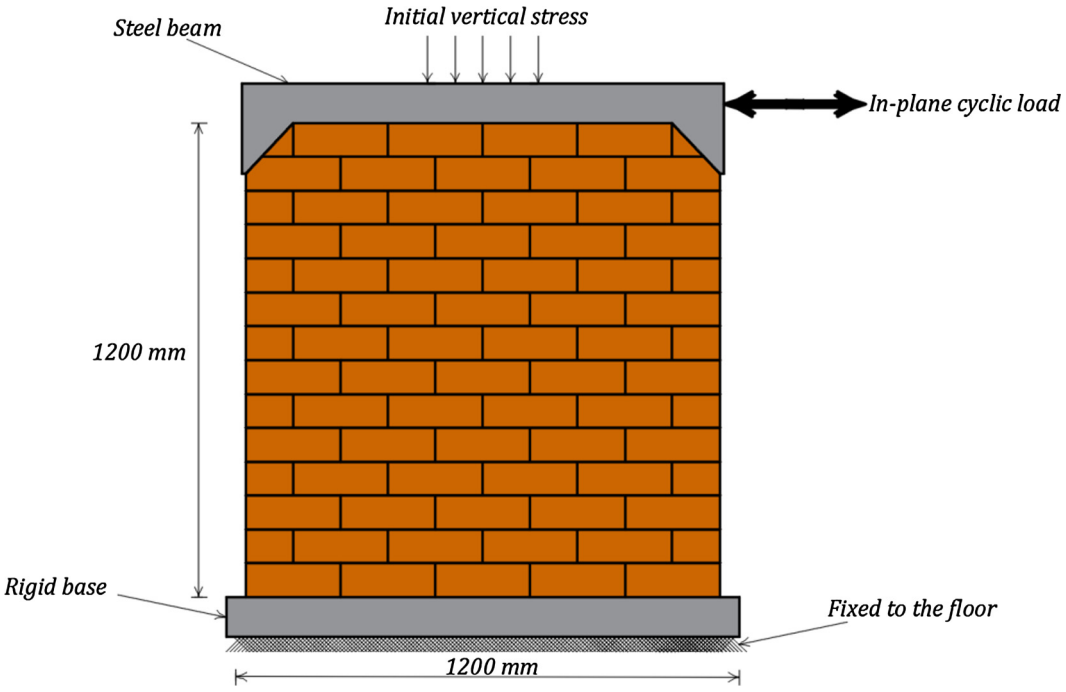

Fig. 23. Test setup of the walls (based on [37]).

Table 7
Elastic properties of constitutive materials and joint interfaces for the wall tested under cyclic load.

Brick units		Mortar	Expanded units	Joint interface		
E_u (MPa) (Calculated)	v [28]	E_m (MPa) (Calculated)	E_{adj} (MPa) (from Eq. (20))	K_{nn} (N/mm^3) (From Eq. (2))	K_{ss} (N/mm^3) (From Eq. (3))	K_{tt} (N/mm^3) (From Eq. (3))
5730	0.15	565	2888	63	25	25

Table 8
Non-linear material properties for the joint interface for the wall tested under cyclic load.

Tension		Shear			Compression
t_n^{max} (MPa) (Calculated)	G_{IC} (N/mm) [36]	c (MPa) [37]	μ, [28]	G_{IIC} (N/mm) (assumed based on [4])	σ_c (MPa) [37]
0.20	0.012	0.64	0.75	0.040	14.18

Table 9
Non-linear material properties for the joint interface where the DPC layer presents i.e. in the bed joint between the first and second courses.

Tension		Shear		
t_n^{max} (MPa) (Calculated)	G_{IC} (N/mm) (Calibrated)	c (MPa) [37]	μ, [37]	G_{IIC} (N/mm) (Calibrated)
0.028	0.0010	0.038	0.425	0.0038

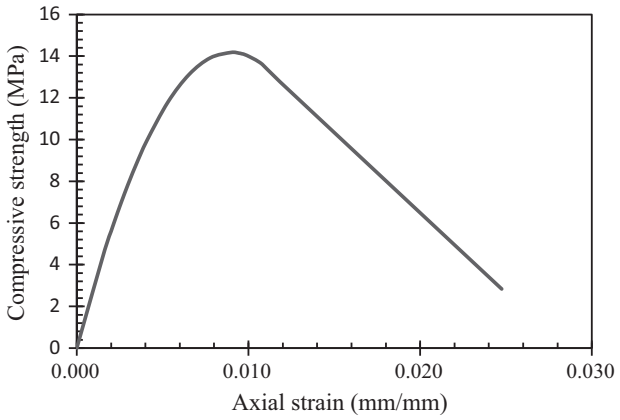

Fig. 25. Compressive stress-strain curve of the masonry walls.

containing the DPC layer. However, it can be noted that the maximum horizontal load attained in the experiment (45.53 kN) is relatively higher than the maximum load in the numerical model (38.94 kN), which indicates that the horizontal crack which propagated in the first bed joint occurred earlier in the numerical model than the experiment. After the propagation of the horizontal crack, the response of the model was governed by the proportional relationship of the coefficient of friction to the normal compressive stresses in the first bed joint. Fig. 26 shows the comparison between the experimental and numerical responses.

In addition, the experimental results showed that the failure mode was due to formation of horizontal cracking along the first bed joint containing the DPC layer and subsequent sliding of the upper part of the wall over the first bed joint. Furthermore, vertical cracks occurred in the first course of the wall as a result of the cyclic sliding movements of the upper part of the wall over the first bed joint Fig. 27(a). Similar failure modes were observed in the numerical results Fig. 27(b) and (c). It is also worth mentioning that the numerical compressive stresses attained were below the compressive strength of the wall during all the cycles Fig. 28, similarly in the experiment no crushing under compression was observed.

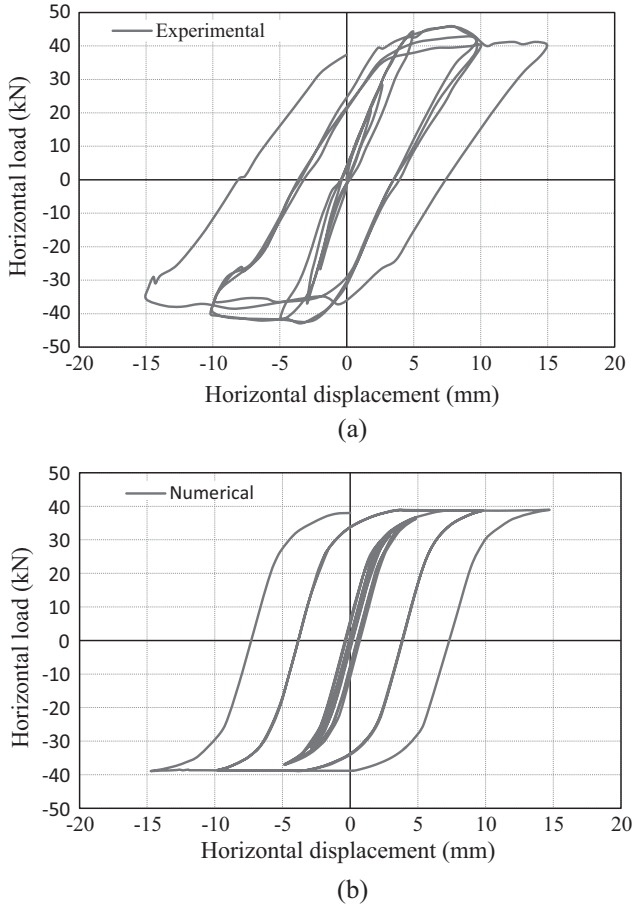

Fig. 26. Comparison between the horizontal force-top wall horizontal displacement responses: (a) experimental, (b) numerical.

5. Conclusions

In this paper a combination of constitutive models has been employed together with the extended finite element method

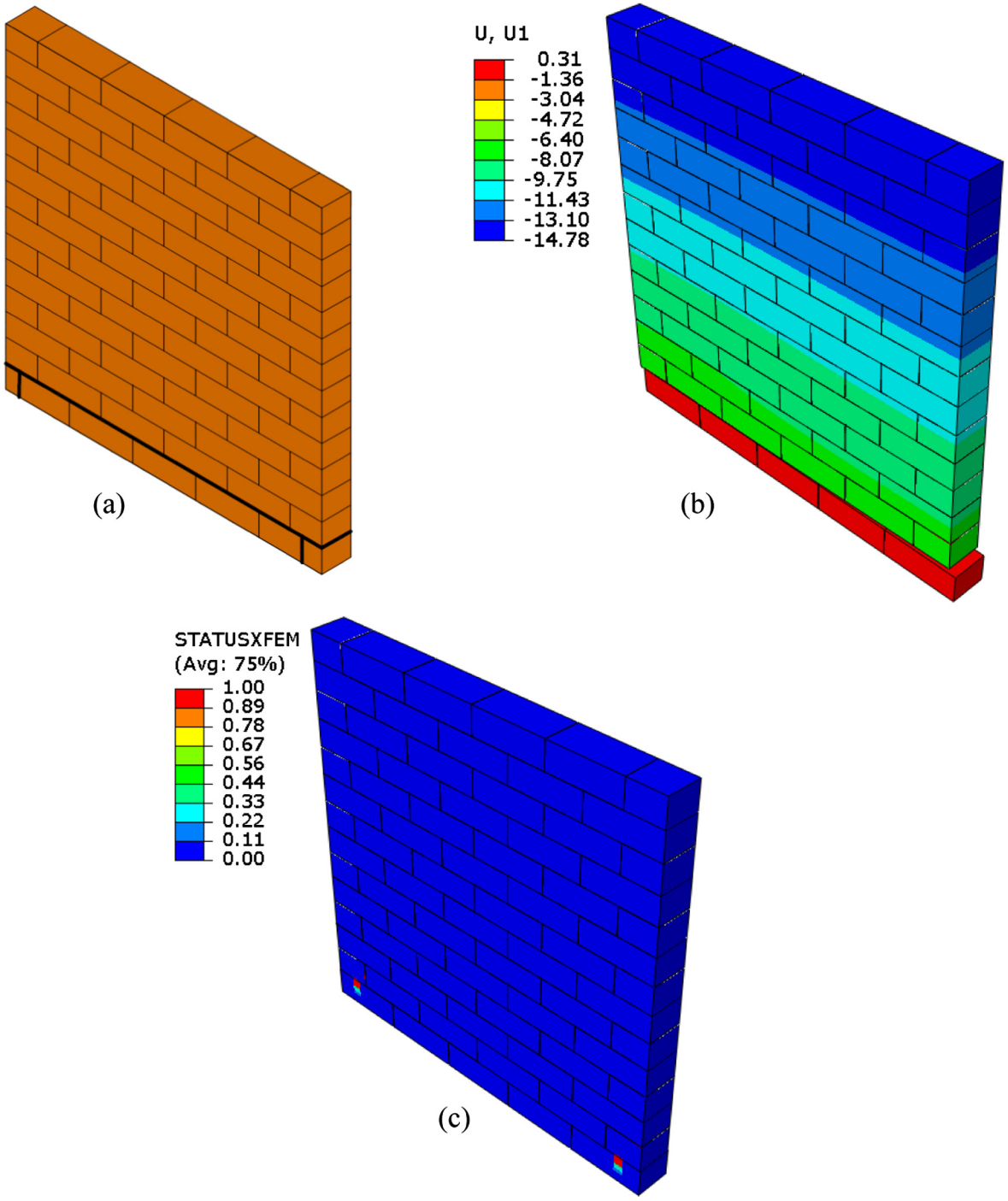

Fig. 27. Comparison between the experimental and numerical failure modes: (a) experimental: sliding over the first bed joint and vertical cracks in the corner bricks in the first bed joint, (b) numerical: cracking of the first bed joint and sliding at the 19th cycle, (c) numerical: STATUSXFEM shows the cracks in the bricks.

(XFEM) to simulate 3D masonry structures using a simplified Micro-modelling approach. In the new approach progressive cracking and non-linear post-failure behaviour between the masonry joint interfaces were well-captured by using a cohesive, surface-based approach with a traction separation law. In addition, crack propagation within masonry units was identified by the novel use of XFEM without the pre-definition of crack location. The compressive failure of masonry was also included via a Drucker-Prager material constitutive model. Thus, all key local and global behaviour and failure modes of masonry were captured. The capability of the proposed model was demonstrated by validation studies of the response of masonry structures under monotonic in-plane, out-of-plane and in-plane cyclic loads, which were able to reproduce experimentally observed behaviour with accuracy and without numerical convergence difficulties.

The approach described has a variety of novel and beneficial features: for the first time masonry structural systems can be modelled in 3D when subject to arbitrary combinations of in-plane and out-of-plane loads without resort to user generated numerical code. This is a significant step forward because it allows masonry to be modelled by practitioners without the resources to develop, and validate, their own code. Moreover, the approach uses a quasi-static solution

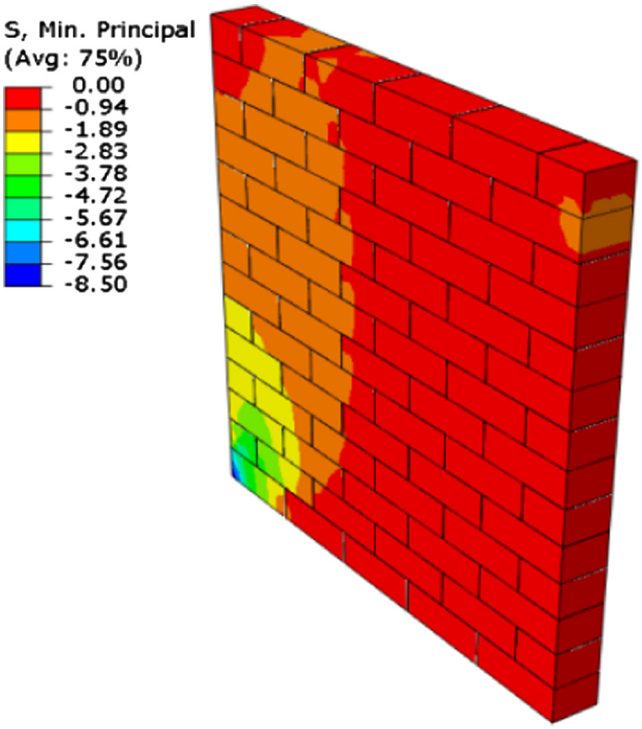

Fig. 28. The distribution of the maximum compressive stresses during the loading history (16th cycle) (N/mm^2).

procedure rather than relying on dynamic-explicit procedures that are onerous to use and interpret. The approach is also the first to capture the cracking of masonry units without the need to specify crack locations in advance, thus removing the need to make significant assumptions, different for each possible load, that are inherent in the approaches available previously. However, the limitation of the proposed model in capturing the failure mode under out-of-plane loads is demonstrated by the fact that multiple distributed cracks rather than single cracks were predicted. This outcome may be due in part to the assumption of uniform properties for unit-mortar interfaces. Further study on the effect of the interface parameters is required. Such further study could include random assignment of varying interface properties across the wall to simulate the variability that occurs in practice.

The approach opens the possibility of analysing complete masonry structures under complex load combinations. It also offers the possibility of examining the efficacy of strengthening systems when applied to masonry structures. Such systems typically require consideration of 3D and out-of-plane behaviour for their effects to be fully captured, something that was previously not so readily possible to obtain numerically. This ability will allow the development and optimisation of strengthening systems without the need for extensive and expensive experimental programmes. This line of research is being pursued by the authors.

Acknowledgements

The authors gratefully acknowledge the Research Impact Scholarship (RIS) at the University of Manchester and the contribution of the University's School of Mechanical, Aerospace and Civil Engineering (MACE) in funding this research.

References

[1] Roca P, Cervera M, Gariup G. Structural analysis of masonry historical constructions. Classical and advanced approaches. Arch Comput Methods Eng 2010;17(3):299–325.
[2] Lourenço PB. Experimental and numerical issues in the modelling of the mechanical behaviour of masonry. Struct Anal Hist Constructions Ii 1998:57–91.
[3] Pandey BH, Meguro K. Simulation of Brick masonry wall behavior under in plane lateral loading using applied element method. In: 13th World conference on earthquake engineering, Vancouver, BC, Canada; August. 2004.
[4] Lourenço PB. Computational strategies for masonry structures. TU Delft: Delft University of Technology; 1996.
[5] Arya S, Hegemier G. On non-linear response prediction of concrete masonry assemblies. In: North masonry conference Boulder. Colorado: Masonry Society; 1978.
[6] Page AW. Finite element model for masonry. J Struct Div 1978;104 (8):1267–85.
[7] Lotfi HR, Shing PB. Interface model applied to fracture of masonry structures. J Struct Eng 1994;120(1):63–80.
[8] Lourenço PB, Rots JG. Multisurface interface model for analysis of masonry structures. J Eng Mech 1997;123(7):660–8.
[9] Shing P, Cao L. Analysis of partially grouted masonry shear walls. US Department of Commerce, Gaithenburg, MD20899. NIST GCR; 1997. p. 97–710.
[10] Sutcliffe D, Yu H, Page A. Lower bound limit analysis of unreinforced masonry shear walls. Comput Struct 2001;79(14):1295–312.
[11] Citto C. Two-dimensional interface model applied to masonry structures. ProQuest; 2008.
[12] Kumar N, Amirtham R, Pandey M. Plasticity based approach for failure modelling of unreinforced masonry. Eng Struct 2014;80:40–52.
[13] Oliveira DV, Lourenço PB. Implementation and validation of a constitutive model for the cyclic behaviour of interface elements. Comput Struct 2004;82 (17):1451–61.
[14] Miglietta PC, Bentz EC, Grasselli G. Finite/discrete element modelling of reversed cyclic tests on unreinforced masonry structures. Eng Struct 2017;138:159–69.
[15] Kuang JS, Yuen Y. Simulations of masonry-infilled reinforced concrete frame failure. Proc Inst Civ Eng – Eng Comput Mech 2013;166(4):179.
[16] La Mendola L et al. Nonlinear FE analysis of out-of-plane behaviour of masonry walls with and without CFRP reinforcement. Constr Build Mater 2014;54:190–6.
[17] Aref AJ, Dolatshahi KM. A three-dimensional cyclic meso-scale numerical procedure for simulation of unreinforced masonry structures. Comput Struct 2013;120:9–23.
[18] Campilho RD, De Moura M, Domingues J. Using a cohesive damage model to predict the tensile behaviour of CFRP single-strap repairs. Int J Solids Struct 2008;45(5):1497–512.
[19] Camanho PP, Dávila CG. Mixed-mode decohesion finite elements for the simulation of delamination in composite materials; 2002.
[20] Benzeggagh M, Kenane M. Measurement of mixed-mode delamination fracture toughness of unidirectional glass/epoxy composites with mixed-mode bending apparatus. Compos Sci Technol 1996;56(4):439–49.
[21] Belytschko T, Black T. Elastic crack growth in finite elements with minimal remeshing. Int J Numer Meth Eng 1999;45(5):601–20.
[22] Melenk JM, Babuška I. The partition of unity finite element method: basic theory and applications. Comput Methods Appl Mech Eng 1996;139(1–4):289–314.
[23] Moes N, Dolbow J, Belytschko T. A finite element method for crack growth without remeshing. Int J Numer Meth Eng 1999;46(1):131–50.
[24] Remmers J, de Borst R, Needleman A. A cohesive segments method for the simulation of crack growth. Comput Mech 2003;31(1–2):69–77.
[25] Drucker DC, Prager W. Soil mechanics and plastic analysis or limit design. Q Appl Math 1952;10(2):157–65.
[26] Lubarda VA, Mastilovic S, Knap J. Brittle-ductile transition in porous rocks by cap model. J Eng Mech 1996;122(7):633–42.
[27] ABAQUS, online documentation. SIMULIA Inc.; 2013.
[28] Raijmakers T, Vermeltfoort AT. Deformation controlled tests in masonry shear walls; 1992.
[29] Mosalam K, Glascoe L, Bernier J. Mechanical properties of unreinforced brick masonry section-1. Documented to US Department of Energy by Lawrence Livermore National Laboratory; 2009.
[30] Kaushik HB, Rai DC, Jain SK. Stress-strain characteristics of clay brick masonry under uniaxial compression. J Mater Civ Eng 2007;19(9):728–39.
[31] Griffith M, Vaculik J. Out-of-plane flexural strength of unreinforced clay brick masonry walls. TMS J 2007;25(1):53–68.
[32] Standard B. Eurocode 6—design of masonry structures—. London: British Standard Institution; 2005.
[33] Milani G, Lourenço P, Tralli A. Homogenization approach for the limit analysis of out-of-plane loaded masonry walls. J Struct Eng 2006;132(10):1650–63.
[34] Willis C, Griffith M, Lawrence S. Horizontal bending of unreinforced clay brick masonry. British Masonry Society; 2004.
[35] Willis C, Griffith M, Lawrence S. Implications of recent experimental and analytical studies for the design of face-loaded URM walls. In: Proceedings of the 7th Australasian masonry conference. University of Newcastle; 2004.
[36] Angelillo M, Lourenço PB, Milani G. Masonry behaviour and modelling. In: Mechanics of masonry structures. Springer; 2014. p. 1–26.
[37] Mojsilović N, Simundic G, Page A. Static-cyclic shear tests on masonry wallettes with a damp-proof course membrane, vol. 319. ETH Zurich; 2009.